Toxicology 469 (2022) 153117

Contents lists available at ScienceDirect

Toxicology

journal homepage: www.elsevier.com/locate/toxicol

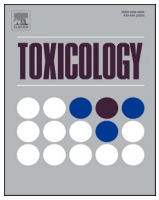

Extracellular histones cause intestinal epithelium injury and disrupt its barrier function *in vitro* and *in vivo*

Chanjuan Chen [a,1], Ziqi Lin [a,*,1], Xiaoxin Zhang [a], Xiaoying Zhang [a], Zhenxing Cheng [b,c], Tao Jin [a], Tingting Liu [a], Lihui Deng [a], Jia Guo [a], Guozheng Wang [b], Qing Xia [a,*]

[a] *Department of Integrated Traditional Chinese and Western Medicine, Sichuan Provincial Pancreatitis Centre and West China-Liverpool Biomedical Research Centre, West China Hospital, Sichuan University, Chengdu, 610041, China*
[b] *The Medical School, Southeast University, Nanjing, 210009, China*
[c] *Department of Gastroenterology, the First Affiliated Hospital of Anhui Medical University, Hefei, 230032, China*

ARTICLE INFO

Handling Editor: Mathieu Vinken

Keywords:
Extracellular histones
Intestinal epithelium
Cell death
Toxicity
Tight junction protein
Intestinal barrier

ABSTRACT

Extracellular histones are cytotoxic to various cells and have been extensively proven a vital mediator of multiple organ injuries. However, the effect of extracellular histones on the intestine remains largely unknown. This study aimed to clarify the effect of extracellular histones on the intestine. IEC-6, a cell line of rat small intestinal epithelial crypt, and C57BL/6 or ICR mice were treated with histones. The IEC-6 cells treated with histones from 20 μg/mL to 200 μg/mL for 0−24 h displayed a decline of cell viability and an increase of cell death in a concentration- and time-dependent manner. Moreover, histones (100 μg/mL) induced IEC-6 apoptosis through activating caspase 3 and necroptosis through up-regulation of receptor-interacting serine/threonine protein kinase 1 and 3 (RIPK1 and RIPK3), phosphorylated mixed-lineage kinase domain-like protein (p-MLKL) along with the decrease of caspase-8. Histones treatment disturbed zonular occludens 1 (ZO-1) expression and increased permeability of IEC-6 cell monolayer. *In vivo*, histones 50 mg/kg injection caused mice intestinal edema, loss apex of villus, epithelial lifting down the sides of the villi, and increased neutrophil infiltration. Elevation of serum intestinal fatty acid binding protein (I-FABP), D-lactate, or Diamine oxidase (DAO) and loss of tight junction protein, ZO-1, at 3 h and 6 h after histones injection strongly indicated severe intestinal epithelium injury, which led to increased permeability of the intestine. In conclusion, extracellular histones cause intestinal epithelial damage *via* direct cytotoxicity. Consequently, intestinal epithelial tight junction and barrier integrity are disrupted, which may play pivotal roles in diverse diseases.

1. Introduction

Endogenous molecules released from distressed or damaged cells -termed damage-associated molecular patterns (DAMPs)-initiate innate and adaptive immune responses and lead to sterile inflammation (Gong et al., 2020). DAMPs-induced tissue damage has been extensively studied in multiple diseases, including trauma (Relja and Land, 2020), cancer (Hernandez et al., 2016; Krysko et al., 2012), neurodegeneration (Thundyil and Lim, 2015), sepsis (Kang et al., 2015), transplantation (Land et al., 2016), acute pancreatitis (Kang et al., 2014), diabetes mellitus (Shin et al., 2015), inflammatory intestinal disease (Boyapati et al., 2016), and so on. Therefore, DAMPs represent potential diagnostic and therapeutic targets for diverse disorders.

Histones are highly conservative cationic intra-nuclear proteins, which in physiology provide structural stability to chromatin and regulate gene expression (Kornberg, 1974). During extensive damage, histones as a member of DAMPs are released passively through cell death or actively from immune cells as part of neutrophil extracellular traps (Szatmary et al., 2018). Circulating histones are elevated in sepsis (Alhamdi et al., 2015), pancreatitis (Liu et al., 2017), trauma (Abrams et al., 2013), acute liver failure (ALF) (Wen et al., 2016), and acute respiratory distress syndrome (ARDS) (Lv et al., 2017), and correlate with disease severity in ALF, ARDS, and pancreatitis (Cheng et al., 2019; Liu et al., 2017; Wen et al., 2016). The median value of circulating histones ranges from 5.6 μg/mL to 63.5 μg/mL (Abrams et al., 2013; Alhamdi et al., 2015; Liu et al., 2017; Lv et al., 2017; Wen et al., 2016).

* Corresponding authors.
E-mail addresses: linziqi_85@163.com (Z. Lin), xiaqing@medmail.com.cn (Q. Xia).
[1] Chanjuan Chen and Ziqi Lin contributed to the work equally.

https://doi.org/10.1016/j.tox.2022.153117
Received 7 January 2022; Received in revised form 29 January 2022; Accepted 1 February 2022
Available online 2 February 2022

Extracellular histones induce tissue injury through receptor-dependent and receptor-independent mechanisms. Similar to other DAMPs, extracellular histones activate toll-like receptors (TLR), especially TLR2, TLR4 and TLR9, and NLRP3 inflammasome to induce systematic inflammation (Allam et al., 2014). Strikingly, cationic histones integrate into the negatively charged phospholipid bilayer of cell membranes, altering their permeability, resulting in an influx of calcium ions and cell death (Szatmary et al., 2018). Extracellular histones induce brain (Villalba et al., 2020), heart (Alhamdi et al., 2016), lung (Lefrançais and Looney, 2017; Zhang et al., 2015), liver (Xu et al., 2011), kidney (Nakazawa et al., 2017), and pancreas (Szatmary et al., 2017) injury. However, a rare study has investigated the effect of extracellular histones on the intestine.

The function of the intestinal epithelium includes nutrient absorption, mucosal barrier, and modulation of intestinal immunity (Günther et al., 2013). During homeostasis, the damaged intestinal epithelium promotes regeneration, and the death and regeneration of the intestinal epithelium remain stable (Patankar and Becker, 2020). Dysregulated cell death in the intestinal epithelium destroys the mucosal barrier and has been associated with several disease states, both food allergy, inflammatory bowel diseases, celiac disease, and sepsis-related intestinal injury (Groschwitz and Hogan, 2009; Haussner et al., 2019; Turner, 2009). A previous study demonstrated that histones more than 25 μg/mL induce significant cytotoxicity in mouse small intestinal MODE-K cells (Pemberton et al., 2010). However, the mechanism of extracellular histones on the intestine remains largely unknown. Therefore, we set out for the first time to address the effect of extracellular histones on the intestine and underlying mechanisms by using rat gut-derived IEC-6 cells as a model *in vitro* and mice injected histones as a model *in vivo*.

2. Materials and methods

2.1. Cell culture

Rat intestinal epithelial cell line IEC-6 was purchased from National Biomedical Laboratory Cell Bank and preserved at the Department of Integrated Traditional Chinese and Western Medicine Laboratory of Sichuan University. IEC-6 cells were cultured in Dulbecco's Modified Eagle Medium (DMEM) (Gibco, USA) containing 10 % fetal bovine serum (FBS) (Gibco, USA) at 37 °C under a humidified condition of 95 % air and 5 % CO_2. The 10th to 20th passage cells were used in the experiments. Before the experiments, the medium was replaced with an FBS-free medium.

2.2. Cell viability assay

Cell viability was evaluated using the Cell Counting Kit-8 (CCK-8) assay kit (Beyotime, China). IEC-6 cells (5, 000 cells per well) were plated in 96-well microplates for 24 h, then treated with 20−200 μg/mL histones (Roche, Germany) for 2−24 h. CCK-8 solution (10 %) was added to each well and the cells were incubated at 37 °C for 1−4 h. Optical density values were determined by a microplate reader (BioTek, USA) at 450 nm. Cell viability was expressed as a percentage of the mean value normalized to the control cells.

2.3. Cell death assays

The images of cell death were recorded by Axio Imager 2 epifluorescence microscopy (Zeiss, Germany) by Hoechst 33342 for staining the nuclei and propidium iodide (PI) for assessing plasma membrane rupture. Briefly, IEC-6 cells were plated into 24-well plates at a density of 1×10^5 cells/well. After incubation for 24 h, cells were treated 100 μg/mL histones for 2−6 h at 37 °C. Then incubated with 50 μg/mL Hoechst 33342 (Thermo Fisher, USA) and 10 μg/mL PI for 0.5 h at 37 °C.

2.4. Flow cytometry

Apoptosis and necrosis were assessed with Annexin V-FITC/PI kit (4A Biotech, China) by flow cytometry. IEC-6 cells were seeded in 6-well plates at a concentration of 4×10^5cells/well and incubated for 12 h. Then, the cells were treated with 100 μg/mL histones incubated for 2−6 h at 37 °C. IEC-6 cells were harvested with 0.25 % trypsin, washed with cold phosphate-buffed saline (PBS), collected by centrifugation at 300 *g* for 5 min, and suspended in binding buffer. Separately, 5 μL of Annexin V-FITC and 10 μL of PI were added to the cell suspension for 5 min. The cells were analyzed using a flow cytometer (BD Biosciences, USA).

2.5. Western blot

Expression of necroptosis and apoptosis-related proteins were quantified by western blot. IEC-6 cells (4×10^5 cells per well) were seeded in 6-well plates, treated with 100 μg/mL histones, and harvested at given times. Protein concentration in each sample was measured. Lysates from IEC-6 cells were extracted with RIPA lysis buffer (Beyotime, China) supplemented with protease and phosphatase inhibitor cocktail tablets (Roche, Germany). The total protein concentration was quantified by a BCA kit (Thermo, United States). Lysates were mixed with 5 × SDS-PAGE sample buffer(GenStar, China)and boiled at 95 °C for 8 min. The 20 mg protein was separated on 10 % or 12.5 % SDS-PAGE gels and transferred to a polyvinylidene fluoride membrane. Membranes were blocked with 5 % nonfat milk for 2 h at room temperature and subsequently incubated with the following primary antibodies overnight at 4 °C: cleaved caspase 3 (1:1000, Cell Signaling Technology, USA), caspase 3 (1:1000, Cell Signaling Technology, USA), cleaved caspase 8 (1:1000, Cell Signaling Technology, USA), caspase 8 (1:1000, Cell Signaling Technology, USA), RIPK1 (1:1000, Cell Signaling Technology, USA), RIPK3 (1:1000, Cell Signaling Technology, USA), MLKL (1:1000, Cell Signaling Technology, USA), phosphorylated MLKL (p-MLKL, 1:1000, Thermo Fisher Scientific, USA), GAPDH (1:1000, ZSGB Bio, China). After rinsing with Tris-buffered saline containing Tween 20 (TBST,15 min × 3), the membranes were incubated with a secondary goat anti-rabbit IgG-HRP antibody (1:10000, HuaAn Biotechnology, China) or a goat anti-mouse IgG-HRP antibody (1:10000, Proteintech, China) for 1 h at room temperature. GAPDH was used as the internal housekeeping protein. Immunoreactivity was detected using a chemiluminescence system and quantified using Image J software (Bio-Rad, USA).

2.6. Monolayer paracellular permeability determination

IEC-6 cells (1×10^5 cells per well) were seeded in a Transwell chamber (the membrane area, 0.33 cm^2; pore size, 0.4 μm, Corning, USA) which were placed in 24-well culture plates. FITC-dextran 4000 (Sigma-Aldrich, USA) with a final concentration of 1 mg/mL was added to the upper chamber of Transwell and the flux of FITC-dextran was determined by sampling the lower chamber after being cultured in an incubator protected from light for 2 h. Meanwhile, a series of known concentrations of FITC-dextran was added to a 96-well plate and placed in the incubator protected from light for 2 h. The fluorescence intensity of FITC-dextran was measured using the POLARstar Omega Plate Reader (BMG Labtech, Germany) with excitation and emission wavelengths of 490 and 520 nm, respectively. Obtain a standard curve based on the known concentration of FITC-dextran and the corresponding fluorescence intensity value. The FITC-dextran concentration of lower chamber was calculated by the aforementioned standard curve line. The apparent permeability coefficient (P_{app}) was calculated as follows: $P_{app} = (d_Q / d_t) / A \times C_0$, where d_Q/dt is the FITC-dextran transfer rate, A is the membrane area of the transwell chamber, C_0 is the initial concentration of FITC-dextran in the upper chamber (Xu et al., 2016).

2.7. Immunofluorescence assay

The effect of histones on zonular occludens 1 (ZO-1) expression was examined by immunofluorescence *in vitro* and *in vivo*. The IEC-6 cells (1×10^5 per well) were seeded on coverslips and treated with or without 100 μg/mL histones for 6 h. The intestinal tissue slices or cell-adherent coverslips were fixed with 4 % formaldehyde, blocked with 5 % goat serum (ZSGB-bio, China), and incubated with anti-ZO-1 antibodies (1:100, Abcam, USA) overnight at 4 °C. Tissue or cells were rinsed with PBS and incubated with Alexa Fluor 488 goat anti-rabbit secondary antibody (1:500, Invitrogen, USA) and nucleic acid dye DAPI (1:1000, Sigma-Aldrich, USA). The images were recorded with Olympus IX 83 fluorescence microscope (Olympus, Japan).

2.8. Animals and model

To explore the detrimental effects of extracellular histones on mouse intestine, male C57BL/6 mice weighing 18−20 g were obtained from Dossy experimental animals Co., Ltd (Chengdu, China), with a certificate number of SCXK-2015−030. All mice were acclimated for 1 week under specific pathogen-free conditions before experiments. The animal experiment procedures were conducted by the animal ethics standard of West China Hospital, Sichuan University, Chengdu, China, and obtained ethical approval (no.2021349A).

Model mice were injected with 50 mg/kg histones from the calf thymus in a total volume of 100 μl *via* tail vein. Sham mice were injected with 100 μl of saline as a control. Animals were sacrificed at 3, 6, 12 and 24 h (n = 3–4 mice each time point). Blood was collected by removed eyeball after the mice were completely anesthetized with isoflurane (Reward, China) and the serum samples were stored at -80℃ refrigerators. The small intestinal tissues were harvested 3 cm in length and were collected 10 cm away from the ileum, then fixed in 10 % neutral formalin for 24 h to prepare the embedded sections.

For measuring the histones-induced changes of intestinal epithelial permeability, ICR male, 8 weeks old mice were purchased from Beijing Vital River Laboratory Animal Technology and housed with free access to water and food in sterile conditions at the Research Centre of Genetically Modified Mice, Southeast University, Nanjing, China. All procedures were performed according to State laws under License (Jiangsu province, 2151981, to ZXC). Mice (n = 5 per group) injected intravenously with histones (0, 10, 50 mg/kg). After 3 h, mice were anesthetized with intraperitoneal injection of ketamine 100 mg/kg, and xylazine 10 mg/kg. A midline laparotomy was then performed to isolate a 5 cm segment of the distal ileum using silk ties. An intraluminal injection of 0.5 mL FITC-dextran 4000 (20 mg/mL in PBS). After 30 min, blood was obtained *via* cardiac puncture to citrated Eppendorf tubes and immediately centrifuged at 10,000 *g* for 10 min to isolate the plasma. The fluorescent intensity of FITC-dextran in plasma was detected using a SpectraMax M5 fluorescence spectrophotometer (excitation, 488 nm; emission, 525 nm). The concentration of FITC-dextran was calculated based on the standard curve generated by serial dilutions of FITC-dextran. Mice were euthanized by neck dislocation.

The animal experiments followed ARRIVE guidelines. The minimal sample sizes in the experimental group were calculated for a power of 80 % and significance of 5 % using values that have been determined in our previous or pilot experiments and animals were randomized to each group.

2.9. Histological examination

Formalin-fixed, paraffin-embedded intestinal tissue samples were sectioned 4 μm, deparaffinized, and stained with hematoxylin and eosin. The images were recorded with Olympus IX 83 microscope (Olympus, Japan). The histopathology changes were examined and classified based on Chiu's score (Chiu et al., 1970) by two persons. The scoring criteria in detail are as follows: (1) Grade 1, normal mucosal villi; (2) Grade 2, development of congestion; (3) Grade 3, an extension of the subepithelial space with the moderate lifting of epithelial layer from the lamina propria; (4) Grade 4, massive epithelial lifting down the sides of villi; (5) Grade 5, denuded villi with lamina propria and dilated capillaries exposed; (6) Grade 6, digestion and disintegration of lamina propria, hemorrhage, and ulceration.

2.10. Immunohistochemical staining

For immunohistochemical staining, endogenous peroxidase was quenched with 3 % methanol-H_2O_2 for 10 min at room temperature. After rinsing with PBS, the antigen was retrieved in a microwave oven by boiling in 10 mmol/L citrate buffer (pH 6.0), followed by washing with PBS. Subsequently, the slides were blocked with 5 % goat serum (ZSGB-bio, China), incubated with anti - myeloperoxidase (MPO) antibodies (1:100 dilution, Abcam, USA) overnight at 4 °C and incubated goat anti-rabbit horseradish peroxidase-conjugated secondary antibody (ZSGB-bio, China) at room temperature. Images of the slides were observed and photographed under a microscope (Olympus IX83, Japan).

2.11. Serum indexes measurements

Intestinal fatty acid binding protein (I-FABP) concentration was determined using the mouse I-FABP ELISA kit (Nanjing Senbeijia, China). D-lactate concentration was measured using the D-Lactate Colorimetric Assay Kit (Sigma-Aldrich, USA). Diamine oxidase (DAO) activity was measured using the DAO assay kit (Nanjing Jiancheng, China). All operations were in accordance with the manufacturer's instructions.

2.12. Statistical analysis

All values were presented as mean ± standard error of mean (SEM). The data were analyzed for statistical significance using IBM SPSS Statistics, version 23.0. Comparisons between two groups were assessed using a two tailed Student's t-test, and comparisons between multiple groups were assessed using a one-way analysis of variance followed by the Turkey post hoc test (if equal variances assumed) or Games-Howell post hoc test (if equal variances not assumed). A P-value < 0.05 was considered to be statistically significant.

3. Results

3.1. Extracellular histones decreased cell viability and induced cell death in IEC-6 cells in a concentration- and time-dependent manner

To characterize the toxic effects of extracellular histones at concentrations from 0 to 200 μg/mL on IEC-6 cells, CCK-8 kit was used. We found that histones reduced cell viability in a concentration-dependent manner (Fig. 1A). Histones at a concentration of 20 μg/mL did not obviously affect IEC-6 cell viability, whilst at 100 μg/mL, the cell viability decreased more than 50 % after 6 h incubation compared to control (Fig. 1A). PI staining showed histones-induced enrichment of PI inside the cells, indicating the loss of plasma membrane integrity and potential cell death (Fig. 1C).

3.2. Extracellular histones induced IEC-6 cells apoptosis and necrosis

To further characterize histones-induced cell death, we used flow cytometry with annexin V-FITC and PI (Fig. 2A). Both annexin V (+) PI (-) representing the population of early apoptotic cells (Fig. 2B), and annexin V (+) PI (+) representing lately apoptosis and potential necrosis were significantly increased after histones (100 μg/mL) treatment (Fig. 2C). Using western blot we found that histones induced caspase 3 cleavage in a time dependent manner (Fig. 2D, 2E). However, both cleaved caspase 8 and caspase 8 decreased after histones treatment

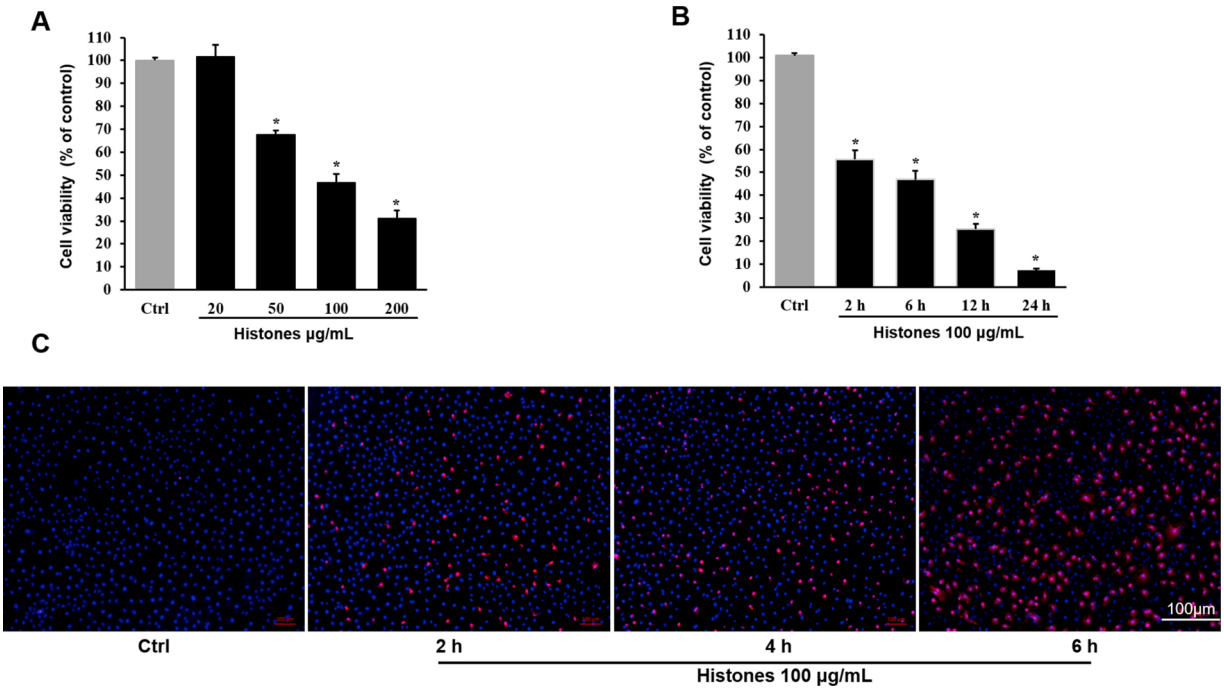

Fig. 1. The toxic effects of extracellular histones on IEC-6 cells in a concentration- and time-dependent manner. (A and B) Cell viability assessed by CCK-8 cell viability kit. **(A)** IEC-6 cells were treated with a serial concentration of histones (0–200 μg/mL) for 6 h or **(B)** with 100 μg/mL histones for 0–24 h. Mean ± SEM from 3 independent experiments is presented. *ANOVA test $P < 0.05$ compared to control (Ctrl). **(C)** IEC-6 cells were incubated with 100 μg/mL histones and PI for determination of cell death, and then fixed and further stained with Hoechst 33342. Representative images were shown. Scale bar = 100 μm. Ctrl: control group.

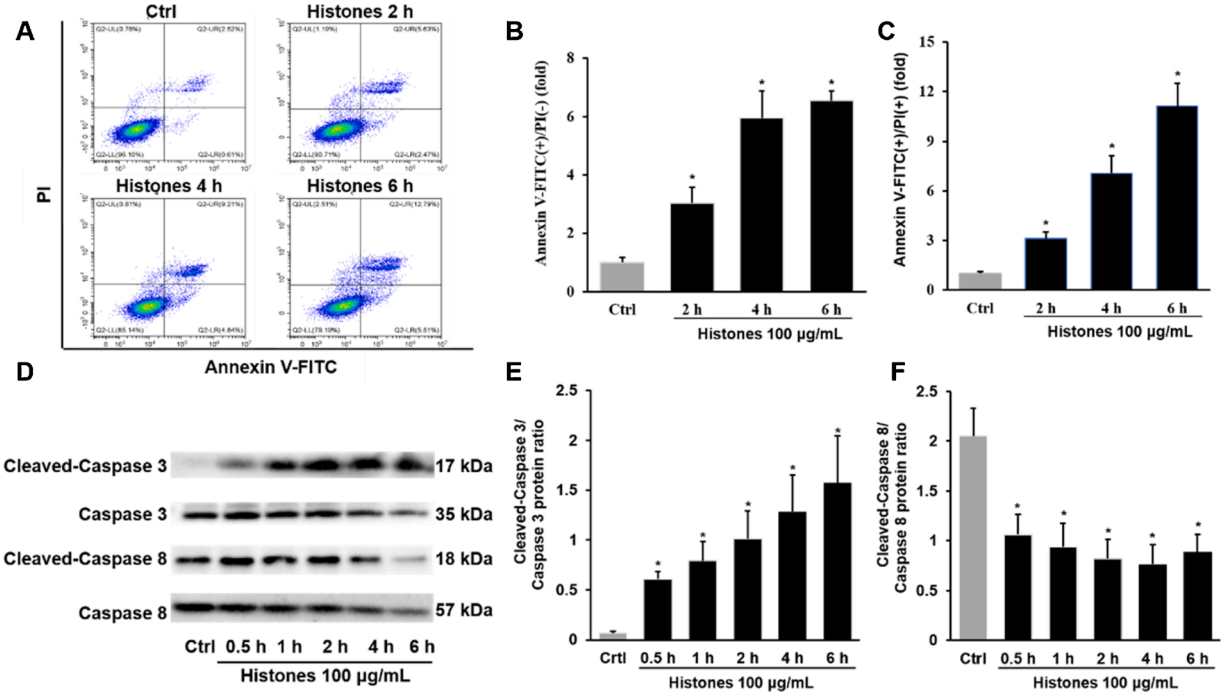

Fig. 2. Extracellular histones induced IEC-6 cells apoptosis. IEC-6 cells were incubated with 100 μg/mL histones for 0–6 h. **(A)** Representative flow chart of Annexin V-FITC/PI double-staining flow cytometry. **(B)** Quantification of apoptosis rates and **(C)** necrosis rates, mean ± SEM (n = 5) are presented. *ANOVA test $P < 0.05$, compared to control group (Ctrl). **(D)** Representative images western blot of cleaved-caspase 3, caspase 3, cleaved-caspase 8, caspase 8 protein in IEC-6 cells incubated with 100 μg/mL histones. **(E)** Cleaved-caspase 3/caspase 3 ratios and **(F)** Cleaved-caspase 8/caspase 8 ratios. Mean ± SEM (n = 5). *ANOVA test $P < 0.05$ compared to control group (Ctrl).

(Fig. 2D). In contrast, the cleaved caspase 8/caspase 8 ratios decreased after the incubation with histones (Fig. 2F).

3.3. Extracellular histones induced IEC-6 cell necroptosis

Necroptosis is also a programmed cell death that is distinct from apoptosis, and mainly mediated by RIPK1, RIPK3 and MLKL (Weinlich et al., 2017). In this study, we used western blot and measured RIPK1, RIPK3 and p-MLKL in IEC-6 cells treated with or without histones (Fig. 3A, 3B). We found that RIPK1 slightly increased, but RIPK3 and p-MLKL obviously elevated in the histones-treated IEC-6 cells compared to the control (Fig. 3C–E).

3.4. Extracellular histones disrupted the tight junction and increased permeability of the monolayer of IEC-6 cells

IEC-6 cells were seeded in chamber slides. On the 11th day, the cells fused to a dense monolayer (data not shown). Tight junction protein, ZO-1, was visualized using immunofluorescence and showed that tight connections between cells developed (Fig. 4A). After incubation with 100 μg/mL histones, the tight junction was disrupted (Fig. 4A). Using Transwell, the permeability of the dense monolayer to FITC-dextran 4000 was measured. Histones significantly increased their permeability (Fig. 4B).

3.5. Infusion histones to mice caused intestinal injury

To further assess the detrimental role of histones *in vivo*, we investigated the histopathological and functional changes in the intestine of mice injected with 50 mg/kg of histones. Histological analysis revealed intestinal edema, loss in the apex of the villus, massive epithelial lifting down the sides of the villi (Fig. 5A), and a significant increase in inflammatory cell infiltration in the lamina propria as revealed by immunostaining with the neutrophil's marker, myeloperoxidase (MPO) (Fig. 5B). MPO staining became more obvious at 3 h and 6 h after histones injection (Fig. 5B). The intestinal histopathology scores in the histones-treated group were markedly higher than that in the control group (Fig. 5C). The intestinal impairment also peaked at 3 h and 6 h after injection and then subsided with time (Fig. 5C). In line with these morphological findings, serum I-FABP and D-lactate levels were significantly elevated at 3 h and 6 h after injection when compared to levels in the sham mice (Fig. 5D and E). Serum DAO level had a similar trend with serum I-FABP and D-lactate, but there is no statistically significance (Fig. 5F).

3.6. Infusion of histones disrupted tight junction and intestinal barrier function in mice

Immunofluorescence of mice intestine showed that histones-treated mice had much less ZO-1 than control mice, suggesting histones infusion could inhibit tight junction protein ZO-1 expression. The expression peaked at 3 h and 6 h after injection, but returned to near normal levels at the 24 h (Fig. 6A). To investigate if any permeability increased after histones infusion, histones were intravenously injected to 3 groups of mice (0, 10, and 50 mg/kg body weight, 5 mice per group). After 3 h, 0.5 mL FITC-dextran 4000 was injected into the lumen of a 5 cm isolated ileum. After 30 min, blood was taken and the fluorescent intensity of FITC-dextran in plasma was measured. We found that histones-infusion significantly increased the intestinal permeability to FITC-dextran 4000 (Fig. 6B), suggesting that histones infusion disrupted mouse intestinal barrier function.

4. Discussion

This study demonstrates that extracellular histones cause intestinal epithelium injury and disrupt its barrier function *in vitro* and *in vivo*. Extracellular histones decreased cell viability and induced cell death in IEC-6 cells in a concentration- and time-dependent manner, which is similar to other reports using different cells (Szatmary et al., 2018). Further investigation, we found that histone-induced IEC-6 cell death mode involved necrosis, apoptosis, and necroptosis. Histones infusion to mice caused intestinal mucosa damage and increase neutrophil infiltration. Extracellular histones also disturb tight junction of intestinal epithelium and disrupt intestinal barrier integrity to increase permeability, an important pathological process in many human diseases.

Extracellular histones are toxic to different cell types of epithelial,

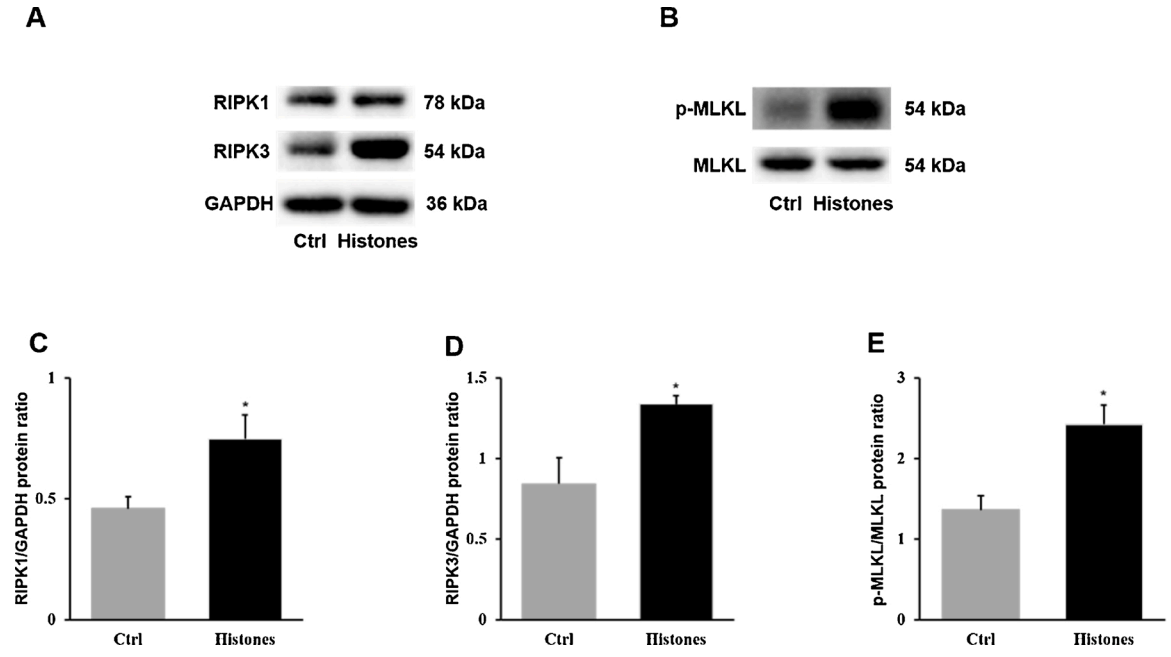

Fig. 3. Extracellular histones induced IEC-6 cells necroptosis. (A and B) Representative images western blot of RIPK1, RIPK3, p-MLKL, MLKL in IEC-6 cells incubated with 0 or 100 μg/mL histones for 6 h. **(C–E)** Quantification of protein expression of western blot of RIPK1/GAPDH ratios, RIPK3/GAPDH ratios and p-MLKL/MLKL ratios. Data are expressed as mean ± SEM from 3 independent experiments. *Student's t test, $P < 0.05$ compared to control group (Ctrl).

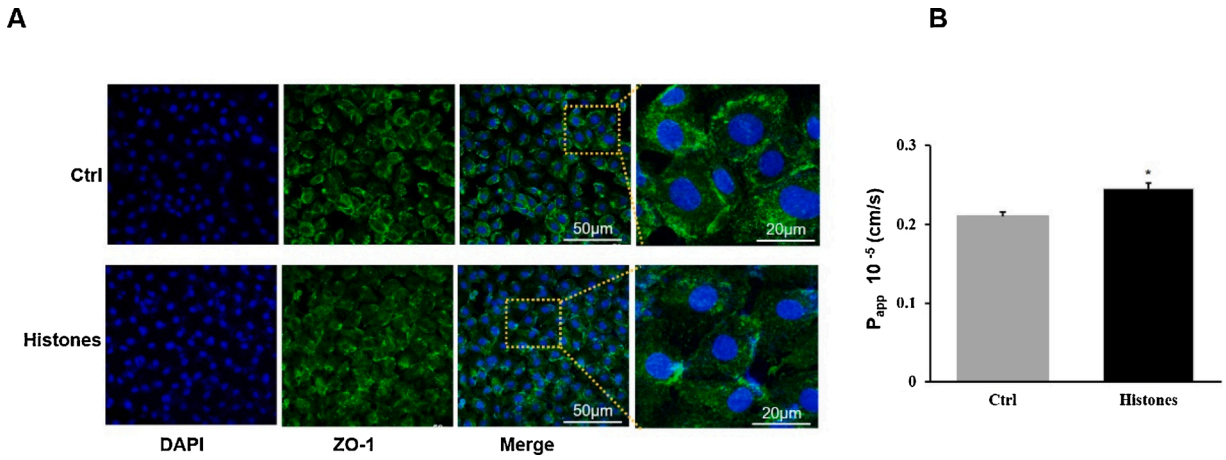

Fig. 4. Effects of histones on the barrier function in IEC-6 cells. The IEC-6 cells were continuously cultured in Transwell chamber, and FITC-dextran concentration of the culture medium in the lower chamber was measured on the 2, 4, 8, 10 days using fluorescent microplate reader. When the cells merged to a dense monolayer, add 100 μg/mL histones and incubate for 6 h, then measure FITC-dextran concentration. **(A)** Immunofluorescence analysis of ZO-1 in IEC-6 treated with 100 μg/mL histones. Nuclei were stained using DAPI (blue). scale bar = 50 μm or 20 μm. **(B)** The apparent permeability coefficient (P_{app}) between control group and histones-treated group. Data are showed as mean ± SEM, n = 4. *Student's t test, $P < 0.05$, compared to control group (Ctrl).

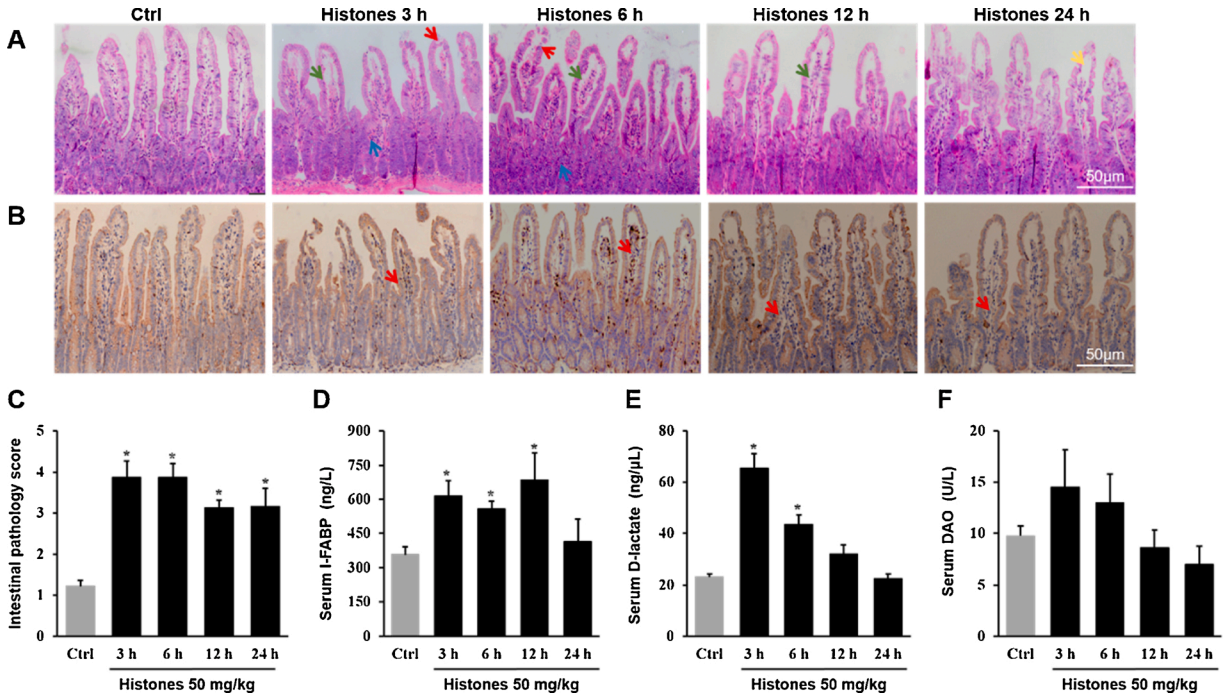

Fig. 5. Infusion histones to mice causes intestinal injury. C57BL/6 mice were injected with histone 50 mg/kg *via* the tail vein and sacrificed on the 3, 6, 12, and 24 h. **(A)** Morphological changes of H&E-stained intestinal sections from mice at different time points after histones infusion. Scale bar = 50 μm. Yellow arrows indicate the Gruenhagen's gap under the apex of the villus is enlarged; green arrow indicates the separation of the epithelial layer and the lamina propria to the ends of the villus; red arrow indicates the dullness or damage of the epithelium; blue arrows indicate inflammatory cell infiltration. **(B)** MPO immunohistochemical staining. Red arrows indicate neutrophils. **(C)** Pathological scores of intestinal tissues by Chiu's score. **(D)** Serum I-FABP. **(E)** Serum D-lactate. **(F)** Serum DAO. Values are expressed as mean ± SEM, n = 3–4. *ANOVA test $P < 0.05$, compared to control group (Ctrl).

endothelial and mesenchymal owing to charge-dependence (Szatmary et al., 2018; Xu et al., 2009). In this study, we noticed that extracellular histones decreased cell viability and induced cell death in IEC-6 cells in a concentration- and time-dependent manner. Histones at a concentration of 20 μg/mL is non-toxic to IEC-6 cell, in line with previous results (Pemberton et al., 2010). Incubation of IEC-6 at concentrations of 50 μg/mL and above for histones quickly caused a decrease in cell viability and an increase in cell death. Meanwhile, morphologic analysis by Hoechst/PI stain also revealed that the mode of cell death of IEC-6 treated with histones is mainly necrosis. It was mainly because histones bind to the cell membrane due to charge attraction, destroy the cell membrane structure, trigger calcium influx, and cause cell necrosis (Bosmann et al., 2013; Pereira et al., 1994).

In the past, cell death is divided into necrosis and apoptosis mainly based on morphological hallmarks and protein regulation. With the deepening of research, a variety of new cell death mode have been discovered, which include necroptosis, pyroptosis, autophagy, and ferroptosis (Bedoui et al., 2020; D'Arcy, 2019; Tang et al. 2021). It is now clear that histones cause cell necrosis. Besides, recent investigation demonstrated that histone H3 induces pyroptosis in macrophages(Shi

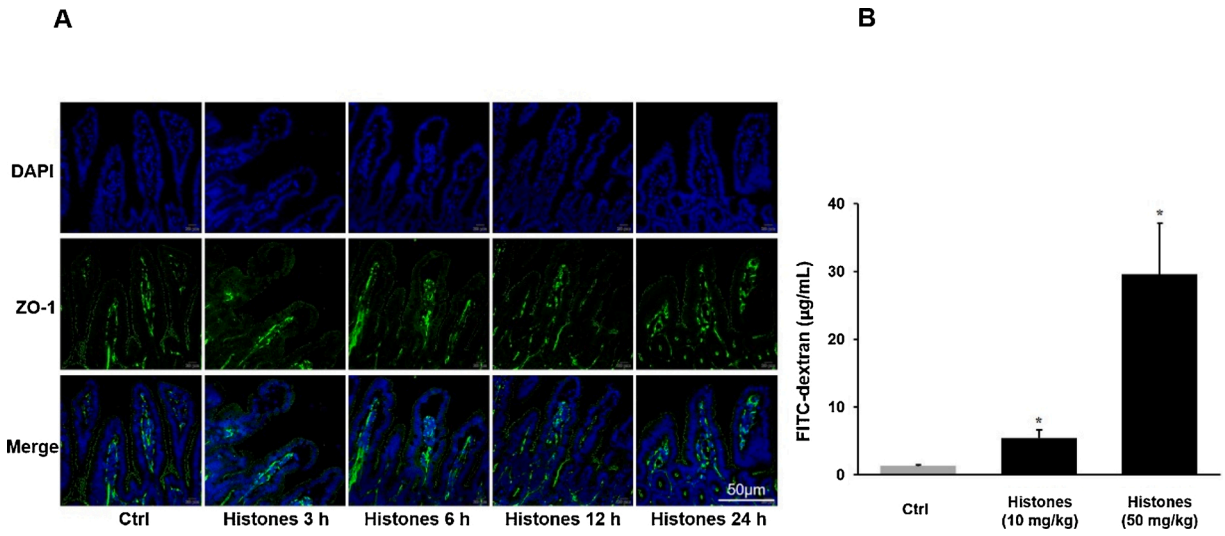

Fig. 6. Histones inhibit tight junction protein ZO-1 expression in intestine and increase intestinal permeability. (A) Immunofluorescence analysis of ZO-1 in mice injected with 50 mg/kg of histones at different points. Nuclei were stained using DAPI (blue). Magnification × 400, scale bar = 50 μm. **(B)** Mouse plasma concentration of FITC-dextran from the lumen of a 5 cm isolated ileum 3 h after intravenous injection of saline, histones (10 mg/kg or 50 mg/kg). Data are expressed as mean ± SEM, n = 5. *ANOVA test $P < 0.01$ compared to control group (Ctrl).

et al., 2020) and hepatocytes (Zhao et al., 2018), autophagy and apoptosis in primary human umbilical vein endothelial cells (Ibañez-Cabellos et al., 2018). Consistent with previous study (Ibañez-Cabellos et al., 2018), histones induce apoptosis in IEC-6 by activating caspase 3. No research has shown the relationship between histones and necroptosis. In this study, our data suggested for the first time that extracellular histones induce necroptosis through activate RIPK1/RIPK3/MLKL and suppress caspase 8 in IEC-6 cells. The intestinal epithelium has one of the highest rates of cellular turnover, while an aberrant increase in the rate of intestinal epithelial cell death underlies instances of extensive epithelial erosion(Patankar and Becker, 2020). Therefore, it is vital to clarify the effect of histones on the death of intestinal epithelial cells.

The intestinal epithelial barrier is maintained by complex protein-protein networks that form desmosomes, adherens junctions and tight junctions (TJs) (Groschwitz and Hogan, 2009). TJ is a component of the apical junctional complex, and it seals paracellular spaces between epithelial cells (Camilleri, 2019). Alterations of TJ protein formation and distribution and/or destabilization of the TJ complexes leads to intestinal epithelial barrier dysfunction. Our data show extracellular histones induce intestinal epithelium death, decreases ZO-1 expression *in vitro* and *in vivo*, furthermore increase intestinal permeability. One limitation of the present study is that we did not investigate the signaling pathways and cannot answer if histones-induced calcium overload or histones-activated TLRs plays the major roles in histones-induced intestinal epithelial cell damage.

Histone-rich NETs have been implicated in multiple intestinal disease pathologies, including enterogenic infections, sepsis-associated gut injury, inflammatory bowel disease, intestinal ischemia-reperfusion injury, and colorectal cancer (Chen et al., 2021). In critical illnesses, circulating histones are elevated after extensive cell death and inflammation activation and cause organ injury *via* direct endothelial/epithelial cytotoxicity, promoting thrombosis and receptor-dependent inflammatory response (Silk et al., 2017; Szatmary et al., 2018). Meantime, the intestinal barrier function is often disrupted, which leads to bacterial translocation to worsen the scenarios (Haussner et al., 2019; He et al., 2019; Otani and Coopersmith, 2019). Using a histones-infusion mouse model to mimic histones release in critical illnesses, we confirmed that extracellular histones play important roles in intestinal injury and permeability changes. This finding holds great potential for anti-histone therapy in the protection of intestinal barrier function to reduce bacterial translocation and its consequence.

5. Conclusion

In conclusion, extracellular histones cause intestinal damage *via* directly intestinal epithelium cytotoxicity, disturb tight junction protein to increase the intestinal permeability.

Funding

This research was funded by National Natural Science Foundation of China (grant number 81503411 to Z.L., 81800575, to T.L.).

Author contributions statement

Chanjuan Chen, Xiaoxing Zhang, Xiaoying Zhang and Ziqi Lin carried out *in vivo* and *in vitro* experiments and data analysis. Zhengxin Cheng carried out part of *in vivo* experiments. Tao Jin, Tingting Liu crried out data analysis. Lihui Deng, Jia Guo and Guozheng Wang revised the manuscript. Ziqi Lin, Guozheng Wang and Qing Xia designed and supervised the study and the manuscript.

Declaration of Competing Interest

The authors declare that they have no conflict of interest.

References

Abrams, S.T., Zhang, N., Manson, J., Liu, T., Dart, C., Baluwa, F., Wang, S.S., Brohi, K., Kipar, A., Yu, W., Wang, G., Toh, C.H., 2013. Circulating histones are mediators of trauma-associated lung injury. American journal of respiratory and critical care medicine 187, 160–169.

Alhamdi, Y., Abrams, S.T., Cheng, Z., Jing, S., Su, D., Liu, Z., Lane, S., Welters, I., Wang, G., Toh, C.H., 2015. Circulating histones are major mediators of cardiac injury in patients with Sepsis. Crit. Care Med. 43, 2094–2103.

Alhamdi, Y., Zi, M., Abrams, S.T., Liu, T., Su, D., Welters, I., Dutt, T., Cartwright, E.J., Wang, G., Toh, C.H., 2016. Circulating histone concentrations differentially affect the predominance of left or right ventricular dysfunction in critical illness. Crit. Care Med. 44, e278–288.

Allam, R., Kumar, S.V., Darisipudi, M.N., Anders, H.J., 2014. Extracellular histones in tissue injury and inflammation. J. Mol. Med. 92, 465–472.

Bedoui, S., Herold, M.J., Strasser, A., 2020. Emerging connectivity of programmed cell death pathways and its physiological implications. Nat. Rev. Mol. Cell Biol. 21, 678–695.

Bosmann, M., Grailer, J.J., Ruemmler, R., Russkamp, N.F., Zetoune, F.S., Sarma, J.V., Standiford, T.J., Ward, P.A., 2013. Extracellular histones are essential effectors of C5aR- and C5L2-mediated tissue damage and inflammation in acute lung injury. FASEB J. 27, 5010–5021.
Boyapati, R.K., Rossi, A.G., Satsangi, J., Ho, G.T., 2016. Gut mucosal DAMPs in IBD: from mechanisms to therapeutic implications. Mucosal Immunol. 9, 567–582.
Camilleri, M., 2019. Leaky gut: mechanisms, measurement and clinical implications in humans. Gut 68, 1516–1526.
Chen, K., Shao, L.H., Wang, F., Shen, X.F., Xia, X.F., Kang, X., Song, P., Wang, M., Lu, X. F., Wang, C., Hu, Q.Y., Liu, S., Guan, W.X., 2021. Netting gut disease: neutrophil extracellular trap in intestinal pathology. Oxid. Med. Cell. Longev. 2021, 5541222.
Cheng, Z., Abrams, S.T., Alhamdi, Y., Toh, J., Yu, W., Wang, G., Toh, C.H., 2019. Circulating histones are major mediators of multiple organ dysfunction syndrome in acute critical illnesses. Crit. Care Med. 47, e677–e684.
Chiu, C.J., McArdle, A.H., Brown, R., Scott, H.J., Gurd, F.N., 1970. Intestinal mucosal lesion in low-flow states. I. A morphological, hemodynamic, and metabolic reappraisal. Arch Surg 101, 478–483.
D'Arcy, M.S., 2019. Cell death: a review of the major forms of apoptosis, necrosis and autophagy. Cell Biol. Int. 43, 582–592.
Gong, T., Liu, L., Jiang, W., Zhou, R., 2020. DAMP-sensing receptors in sterile inflammation and inflammatory diseases. Nat. Rev. Immunol. 20, 95–112.
Groschwitz, K.R., Hogan, S.P., 2009. Intestinal barrier function: molecular regulation and disease pathogenesis. J. Allergy Clin. Immunol. 124, 3–20 quiz 21-22.
Günther, C., Neumann, H., Neurath, M.F., Becker, C., 2013. Apoptosis, necrosis and necroptosis: cell death regulation in the intestinal epithelium. Gut 62, 1062–1071.
Haussner, F., Chakraborty, S., Halbgebauer, R., Huber-Lang, M., 2019. Challenge to the intestinal mucosa during Sepsis. Front. Immunol. 10, 891.
He, W., Wang, Y., Wang, P., Wang, F., 2019. Intestinal barrier dysfunction in severe burn injury. Burns Trauma 7, 24.
Hernandez, C., Huebener, P., Schwabe, R.F., 2016. Damage-associated molecular patterns in cancer: a double-edged sword. Oncogene 35, 5931–5941.
Ibañez-Cabellos, J.S., Aguado, C., Pérez-Cremades, D., García-Giménez, J.L., Bueno-Betí, C., García-López, E.M., Romá-Mateo, C., Novella, S., Hermenegildo, C., Pallardó, F.V., 2018. Extracellular histones activate autophagy and apoptosis via mTOR signaling in human endothelial cells. Biochim Biophys Acta Mol Basis Dis 1864, 3234–3246.
Kang, R., Lotze, M.T., Zeh, H.J., Billiar, T.R., Tang, D., 2014. Cell death and DAMPs in acute pancreatitis. Mol. Med. 20, 466–477.
Kang, J.W., Kim, S.J., Cho, H.I., Lee, S.M., 2015. DAMPs activating innate immune responses in sepsis. Ageing Res. Rev. 24, 54–65.
Kornberg, R.D., 1974. Chromatin structure: a repeating unit of histones and DNA. Science 184, 868–871.
Krysko, D.V., Garg, A.D., Kaczmarek, A., Krysko, O., Agostinis, P., Vandenabeele, P., 2012. Immunogenic cell death and DAMPs in cancer therapy. Nature reviews. Cancer 12, 860–875.
Land, W.G., Agostinis, P., Gasser, S., Garg, A.D., Linkermann, A., 2016. Transplantation and damage-associated molecular patterns (DAMPs). Am. J. Transplant. 16, 3338–3361.
Lefrançais, E., Looney, M.R., 2017. Neutralizing Extracellular Histones in Acute Respiratory Distress Syndrome. A New Role for an Endogenous Pathway. Am. J. Respir. Crit. Care Med. 196, 122–124.
Liu, T., Huang, W., Szatmary, P., Abrams, S.T., Alhamdi, Y., Lin, Z., Greenhalf, W., Wang, G., Sutton, R., Toh, C.H., 2017. Accuracy of circulating histones in predicting persistent organ failure and mortality in patients with acute pancreatitis. Br. J. Surg. 104, 1215–1225.
Lv, X., Wen, T., Song, J., Xie, D., Wu, L., Jiang, X., Jiang, P., Wen, Z., 2017. Extracellular histones are clinically relevant mediators in the pathogenesis of acute respiratory distress syndrome. Respir. Res. 18, 165.
Nakazawa, D., Kumar, S.V., Marschner, J., Desai, J., Holderied, A., Rath, L., Kraft, F., Lei, Y., Fukasawa, Y., Moeckel, G.W., Angelotti, M.L., Liapis, H., Anders, H.J., 2017. Histones and Neutrophil Extracellular Traps Enhance Tubular Necrosis and Remote Organ Injury in Ischemic AKI. J. Am. Soc. Nephrol. 28, 1753–1768.
Otani, S., Coopersmith, C.M., 2019. Gut integrity in critical illness. J. Intensive Care 7, 17.
Patankar, J.V., Becker, C., 2020. Cell death in the gut epithelium and implications for chronic inflammation. Nat. Rev. Gastroenterol. Hepatol. 17, 543–556.
Pemberton, A.D., Brown, J.K., Inglis, N.F., 2010. Proteomic identification of interactions between histones and plasma proteins: implications for cytoprotection. Proteomics 10, 1484–1493.
Pereira, L.F., Marco, F.M., Boimorto, R., Caturla, A., Bustos, A., De la Concha, E.G., Subiza, J.L., 1994. Histones interact with anionic phospholipids with high avidity; its relevance for the binding of histone-antihistone immune complexes. Clin. Exp. Immunol. 97, 175–180.
Relja, B., Land, W.G., 2020. Damage-associated molecular patterns in trauma. Eur. J. Trauma Emerg. Surg. 46, 751–775.
Shi, C.X., Wang, Y., Chen, Q., Jiao, F.Z., Pei, M.H., Gong, Z.J., 2020. Extracellular histone H3 induces pyroptosis during Sepsis and may act through NOD2 and VSIG4/NLRP3 pathways. Front. Cell. Infect. Microbiol. 10, 196.
Shin, J.J., Lee, E.K., Park, T.J., Kim, W., 2015. Damage-associated molecular patterns and their pathological relevance in diabetes mellitus. Ageing Res. Rev. 24, 66–76.
Silk, E., Zhao, H., Weng, H., Ma, D., 2017. The role of extracellular histone in organ injury. Cell Death Dis. 8, e2812.
Szatmary, P., Liu, T., Abrams, S.T., Voronina, S., Wen, L., Chvanov, M., Huang, W., Wang, G., Criddle, D.N., Tepikin, A.V., Toh, C.H., Sutton, R., 2017. Systemic histone release disrupts plasmalemma and contributes to necrosis in acute pancreatitis. Pancreatology 17, 884–892.
Szatmary, P., Huang, W., Criddle, D., Tepikin, A., Sutton, R., 2018. Biology, role and therapeutic potential of circulating histones in acute inflammatory disorders. J. Cell. Mol. Med. 22, 4617–4629.
Tang, D., Chen, X., Kang, R., Kroemer, G., 2021. Ferroptosis: molecular mechanisms and health implications. Cell Res. 31, 107–125.
Thundyil, J., Lim, K.L., 2015. DAMPs and neurodegeneration. Ageing Res. Rev. 24, 17–28.
Turner, J.R., 2009. Intestinal mucosal barrier function in health and disease. Nat. Rev. Immunol. 9, 799–809.
Villalba, N., Baby, S., Cha, B.J., Yuan, S.Y., 2020. Site-specific opening of the blood-brain barrier by extracellular histones. J. Neuroinflammation 17, 281.
Weinlich, R., Oberst, A., Beere, H.M., Green, D.R., 2017. Necroptosis in development, inflammation and disease. Nat. Rev. Mol. Cell Biol. 18, 127–136.
Wen, Z., Lei, Z., Yao, L., Jiang, P., Gu, T., Ren, F., Liu, Y., Gou, C., Li, X., Wen, T., 2016. Circulating histones are major mediators of systemic inflammation and cellular injury in patients with acute liver failure. Cell Death Dis. 7, e2391.
Xu, J., Zhang, X., Pelayo, R., Monestier, M., Ammollo, C.T., Semeraro, F., Taylor, F.B., Esmon, N.L., Lupu, F., Esmon, C.T., 2009. Extracellular histones are major mediators of death in sepsis. Nat. Med. 15, 1318–1321.
Xu, J., Zhang, X., Monestier, M., Esmon, N.L., Esmon, C.T., 2011. Extracellular histones are mediators of death through TLR2 and TLR4 in mouse fatal liver injury. J. Immunol. 187, 2626–2631.
Xu, S., Xue, X., You, K., Fu, J., 2016. Caveolin-1 regulates the expression of tight junction proteins during hyperoxia-induced pulmonary epithelial barrier breakdown. Respir. Res. 17, 50.
Zhang, Y., Wen, Z., Guan, L., Jiang, P., Gu, T., Zhao, J., Lv, X., Wen, T., 2015. Extracellular histones play an inflammatory role in acid aspiration-induced acute respiratory distress syndrome. Anesthesiology 122, 127–139.
Zhao, H., Huang, H., Alam, A., Chen, Q., Suen, K.C., Cui, J., Sun, Q., Ologunde, R., Zhang, W., Lian, Q., Ma, D., 2018. VEGF mitigates histone-induced pyroptosis in the remote liver injury associated with renal allograft ischemia-reperfusion injury in rats. Am. J. Transplant. 18, 1890–1903.